ACS APPLIED MATERIALS & INTERFACES

Letter

www.acsami.org

Preparation of Super-Stable Gold Nanorods via Encapsulation into Block Copolymer Micelles

Dae Hwan Kim,[†] Alexander Wei,[‡] and You-Yeon Won*,[†]

[†]School of Chemical Engineering and [‡]Department of Chemistry, Purdue University, West Lafayette, Indiana 47907, United States

Supporting Information

ABSTRACT: Gold nanorods (GNRs) have the potential to be used as imaging and hyperthermia agents for cancer theranostics. Clinical applications of as-synthesized GNRs (i.e., cetyl trimethylammonium bromide (CTAB)-coated GNRs) are currently limited by their cytotoxicity and insufficient colloidal stability. With an aim to address these problems, we developed a self-assembly processing technique for encapsulating GNRs in poly(ethylene oxide)-poly(*n*-butyl acrylate) (PEO-PnBA) block copolymer (BCP) micelles. This technique uses simple steps of solvent exchange processes, based on the known principles of block copolymer self-assembly. The resultant BCP-encapsulated GNRs were found to be stable against aggregation under physiological salt conditions for indefinite periods of time, which has rarely previously been achieved by other means of encapsulation.

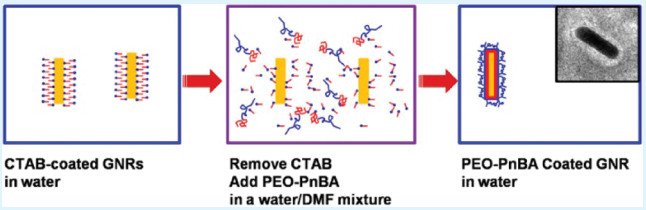

KEYWORDS: *gold nanorod, stabilization, block copolymer, micelle, encapsulation, CTAB*

1. INTRODUCTION

Gold nanorods (GNRs) are promising candidates for use as contrast agents for medical imaging because they exhibit tunable surface plasmon resonances (SPR) by control of their size and aspect ratio.[1−4] In particular, the optical resonances of GNRs can be tuned to a near-infrared (NIR) wavelength range (i.e., $\lambda \approx 650-900$ nm) where light has its maximum depth of penetration in biological tissue.[1] GNRs can also be used as photothermal transducers for the hyperthermic treatment of cancer, as the absorption of NIR photons decays mostly through phonon emission (i.e., heat).[1,5,6] The standard synthesis technique for making GNRs involves a cationic surfactant, cetyl trimethylammonium bromide (CTAB); here, CTAB functions both as a structure-directing agent and also as a capping agent.[7,8] For this reason, as-synthesized GNRs are normally coated with bilayers of CTAB. Unfortunately, clinical applications of these photothermally active nanomaterials are currently limited by the cytotoxicity of CTAB, and also the nonspecific uptake of CTAB-coated GNRs.[9] Simply displacing the CTAB coating from the GNR surface cannot be a solution to this problem, because uncoated GNRs are neither stable nor appropriate for *in vivo* use because of opsonization. It is well-known that improperly passivated GNRs and other nanoparticles can adventitiously alter gene expression upon accumulation in cells and organs,[10] and are also prone to aggregation.[11,12]

To address this limitation, researchers have proposed several strategies for further modification of the surfaces of the GNRs.[1−3,11,13,14] These strategies attempt to replace the original CTAB coating with a new enclosure formed by other materials such as negatively charged lipids, thiolated poly(ethylene oxide) (PEO),[15] alkanethiol derivatives,[11,14] polyelectrolyte multilayers,[16] or silica shells.[17] In particular, the method of conjugation of GNRs with PEO thiols is very common.[1,3,18] However, this method does not normally produce dense PEO brushes because of the steric repulsion between grafted PEO strands.[1,18,19] Incomplete coverage of gold nanoparticles with PEO has been shown to result in insufficient stability of the particles against aggregation.[20] Although alkanethiols are known to form a dense passivation layer on planar gold surfaces,[12] the direct exposure of CTAB-capped GNRs to alkanethiol agents usually results in incomplete removal and replacement of the original CTAB layer.[14,19,21−23] By careful control of experimental parameters[11] or by using PEO thiols as a temporary stabilizing agent during intermediate stages of the CTAB replacement process,[24] it is possible to achieve alkanethiol-encapsulated GNRs that are stable in aqueous media. However, the long-term chemical stability of chemisorbed thiols on gold under physiological conditions[25] remains a concern for in vivo applications of alkanethiol-stabilized GNRs.

In the block copolymer (BCP) community, researchers have recognized the potential of amphiphilic block copolymers as encasing agents for premade nanomaterials (such as various metal/ceramic-based nanostructures or carbon nanotubes).[26] Many block copolymer micelles are highly stable (e.g., critical micellization concentration ≈0),[26−28] making this class of materials suitable for in vivo theranostic applications which require the self-assembled structures to maintain their integrity after exposure to physiological environments. It has been

Received: February 4, 2012
Accepted: March 27, 2012
Published: April 3, 2012

demonstrated that when micellization is induced by solvent exchange in the presence of codispersed gold nanoparticles (>about 10 nm), poly(acrylic acid)-polystyrene (PAA-PS) diblock copolymers form micelle-like aggregates with nanoparticle cores encapsulated within micellar sheaths.[29−32] For iron oxide or zinc sulfide-coated cadmium selenide nanoparticles that are typically much smaller than the chain dimensions of encapsulating block copolymers, both the solvent exchange procedure[33] and the method of direct codissolution of the nanoparticles with amphiphilic block copolymers into water[34,35] have been demonstrated to produce stable block copolymer/nanoparticle assemblies, where the nanoparticles are encapsulated as clusters within the hydrophobic core domains of the block copolymer micelles. The process of encapsulating individual GNRs into BCP micelles for potential medical applications is more challenging, however, because the CTAB coating must be removed from the GNR surface prior to the BCP encapsulation, for reasons mentioned above. Furthermore, the encapsulation of single GNRs within each BCP micelle is desirable in order to fully exploit the unique optical properties of GNRs, as aggregation can cause a shift in their plasmon resonances.[1] In the present report, we will show that the encapsulation of individual GNRs can be practically achieved by means of a self-assembly technique based on simple solvent exchange processes (Scheme 1). In this study, we use a (new) poly(ethylene oxide)-poly(*n*-butyl acrylate) (PEO-PnBA) diblock copolymer as the micelle-forming encapsulation material. The rationale behind the selection of this PEO-PnBA copolymer will be discussed in detail, in particular, in terms of the wetting property of the polymer on the gold surface, which is an issue that, to our knowledge, has not been discussed previously. This PEO-PnBA polymer is also distinguished from the PS-PAA polymer (i.e., the most commonly studied polymer for encapsulation of nanoparticles) by being nonionic, which makes the resultant polymer/nanoparticle assemblies insensitive to changes in the ionic strength of the medium.

Scheme 1. Procedure for Encapsulating Gold Nanorods (GNRs) in Poly(ethylene oxide)−Poly(*n*-butyl acrylate) (PEO-PnBA) Block Copolymer (BCP) Micelles, with Efficient Exchange of CTAB[a]

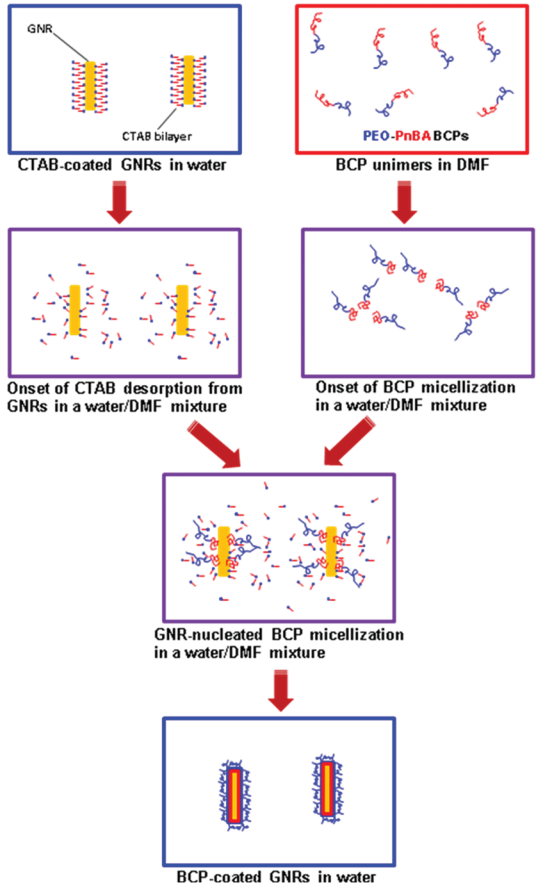

[a]When the micellization is induced by solvent exchange in the presence of codispersed GNRs, PEO-PnBA diblock copolymers form rodlike micelles with GNR cores encapsulated within the micelle shells (bottom figure); the hydrophobic PnBA chains have a strong affinity for the gold-water interface (as explained in Section 2.1) and thus self-assemble into a micelle core domain surrounding the GNR interior; the water-compatible PEO chains form a dense polymer brush layer on the outer surface of the micelle and thus provide colloidal stability to the encapsulated GNR particles even under high ionic strength conditions (demonstrated in Section 2.3).

2. RESULTS AND DISCUSSION

2.1. Rationale for the Choice of Block Copolymer. For demonstrating the concept of encapsulating a gold nanorod (GNR) within a self-assembled block copolymer (BCP) micelle, we used a BCP consisting of a water-soluble PEO segment and a hydrophobic poly(*n*-butyl acrylate) (PnBA) segment. This PEO-PnBA copolymer was chosen based on the following considerations: Considering the potential utility of GNRs in medical applications, PEO was an obvious choice because of its nonionic nature and also its well-known biocompatibility and resistance to protein adhesion. PnBA was selected as the hydrophobic component because it is known to be biologically inert under physiological conditions,[36,37] is liquid-like (i.e., amorphous and nonglassy) at room temperature (T_g = −55 °C),[38] and has a strong tendency to spontaneously wet the gold-water interface (as will be discussed in detail below). Such characteristics not only help to increase the efficiency of encapsulation, but also suppress any lateral inhomogeneities in composition and morphology of the block copolymer coating layer. The tendency of a water-insoluble polymer to wet the gold surface immersed in water can be evaluated by estimation of the polymer's spreading coefficient *s*, defined as $\gamma_{gold-water} - (\gamma_{polymer-gold} + \gamma_{polymer-water})$ where γ_{i-j} denotes the interfacial tension between materials *i* and *j*. If $s > 0$, the polymer will tend to spread and wet the interface in order to reduce the overall interfacial energy; if $s < 0$, the polymer will dewet from the interface. To determine the spreading coefficient of PnBA at the gold-water interface, we conducted contact angle measurements of water on a PnBA surface layer prepared by spin-coating, of water on a freshly prepared gold substrate (prepared by e-beam evaporation), and of PnBA on gold. The static contact angles were measured to be 67.4, 71.7 and ∼0°, respectively. On the basis of these data and literature values for $\gamma_{air-water}$, $\gamma_{PnBA-air}$, and $\gamma_{gold-air}$ (summarized in Table 1), the values of the remaining interfacial tension parameters were estimated: $\gamma_{PnBA-water}$ = 5.6 mJ/m^2, $\gamma_{gold-water}$ = 1477.1 mJ/m^2, and $\gamma_{PnBA-gold}$ = 1466.3 mJ/m^2 (see the table for details). From these values, we were able to calculate the spreading coefficient of PnBA, s = +5.1 mJ/m^2; we note that although the uncertainty in the reported value of $\gamma_{gold-air}$ is orders of magnitude greater than the resultant estimate of *s*, the effects of this uncertainty are canceled out between the $\gamma_{gold-water}$ and

Table 1. Interfacial Tension Values (in units of mJ/m^2) at Room Temperature (A) for the Interfaces Involving Poly(n-butyl acrylate) (PnBA) or Polystyrene (PS) and (B) for Other Interfaces Relevant to the Spreading Coefficient Calculations Discussed in Section 2.1

(A)

polymer	$\gamma_{polymer-gold}$	$\gamma_{polymer-water}$	$\gamma_{polymer-air}$
PnBA	1466.3[a]	5.6[b]	33.7[47]
PS	1460.0[a]	32.4[b]	40.0[48]

(B)

$\gamma_{gold-water}$	$\gamma_{gold-air}$	$\gamma_{air-water}$
1477.1[c]	1500.0[49]	73.0[50]

[a]Calculated using the relation $\gamma_{gold-air} = \gamma_{polymer-gold} + \gamma_{polymer-air}\cos\theta_{polymer/gold}$. Both the contact angles of PnBA and PS on gold ($\theta_{PnBA/gold}$ and $\theta_{PS/gold}$, respectively) were measured to be close to zero. [b]Calculated using the equation $\gamma_{polymer-air} = \gamma_{polymer-water} + \gamma_{air-water}\cos\theta_{water/polymer}$. The contact angle of water on PnBA ($\theta_{water/PnBA}$) was measured to be 67.4°. The reported value of $\theta_{water/PS}$ is 84°.[48] [c]Calculated using the relation $\gamma_{gold-air} = \gamma_{gold-water} + \gamma_{air-water}\cos\theta_{water/gold}$. The contact angle of water on gold ($\theta_{water/gold}$) was measured to be 71.7°.

$\gamma_{PnBA-gold}$ terms in the calculation of the spreading coefficient, resulting in a sufficiently small uncertainty for s. This property of PnBA is in contrast to that of, for example, the common hydrophobic polymer polystyrene (PS) for which, on the basis of available data for γ_{PS-air} and $\gamma_{PS-water}$ (Table 1) and the measured value of the contact angle of PS on gold (≈ 0°, which gives $\gamma_{PS-gold}$ = 1460.0 mJ/m^2), the spreading coefficient is estimated to be negative, i.e., $s = \gamma_{gold-water} - (\gamma_{PS-gold} + \gamma_{PS-water}) = 1477.1 - (1460.0 + 32.4) = -15.3$ mJ/m^2. The PS segments are expected to form isolated aggregates at the gold–water interface in order to reduce the area of the hydrophobic interface in contact with both gold and water.

Equally important to the successful encapsulation of GNRs, as will be demonstrated in Section 2.2, is the appropriate choice of the composition of the copolymer, which is important not just because the specific interfacial curvature preferred by the block copolymer should be commensurate with the geometry of the GNR particle, but also because it determines the range of solvent composition in which the micelle encapsulation process is feasible (as discussed in detail in the next section). This point will be illustrated using two PEO-PnBA diblock copolymers having different block compositions: PEO_{113}–$PnBA_{89}$ and PEO_{113}–$PnBA_{57}$, where the subscripts denote the number-average degrees of polymerization of the individual blocks (determined by ^{1}H NMR spectroscopy).

2.2. Self-Assembly Processing Technique for Encapsulation of GNRs in BCP Micelles via a Solvent Exchange Process. As-synthesized GNRs typically coated by a layer of cationic surfactant, cetyl trimethylammonium bromide (CTAB), which is used in the synthesis of GNRs as a templating and stabilizing agent.[1,7,8] This CTAB coating is thought to assume a bilayer structure under aqueous conditions,[12,39] and is very stable against desorption even at diluted concentrations. In our method, we required CTAB to be removed from the GNR surface just prior to their encapsulation with the BCP, as it compromises the affinity of the gold surface to the BCP. In designing the CTAB removal process, the following factors were taken into account: (i) CTAB forms normal micelles in water at low millimolar concentrations;[40] (ii) CTAB forms reverse micelles in organic solvents, as the quaternary ammonium-bromide ion pair is poorly solvated in aprotic media;[41] (iii) in a binary aqueous–organic solvent mixture, there can exist a window of solvent composition in which both the surfactant tail and head groups become solvated, which can promote the desorption of CTAB from the GNR surface. Specifically, we used dimethylformamide (DMF) as an organic cosolvent to control the partitioning of CTAB between the gold surface and the solution phase. When the DMF weight fraction (w_{DMF}) is above 0.30, CTAB desorbs from the gold surface and induces the aggregation of the uncoated GNR particles (Figure 1). In the DMF-rich

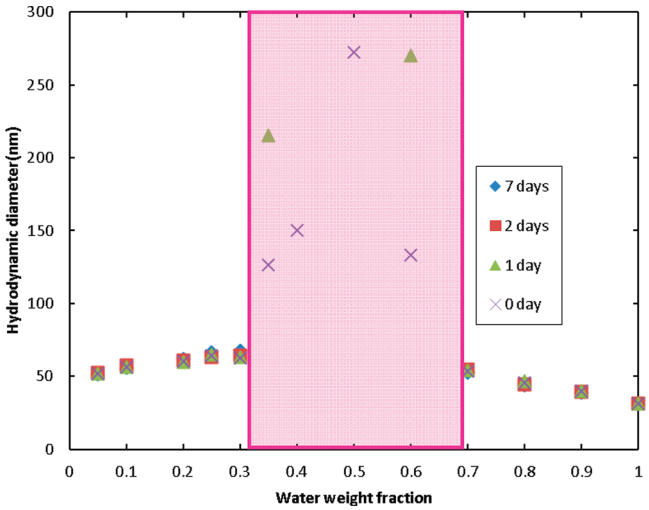

Figure 1. Mean hydrodynamic diameter (measured by DLS) of CTAB-stabilized GNRs in binary water/DMF mixtures as a function of w_{water} and time. The shaded area represents the solvent composition window in which CTAB desorbs from GNRs.

regime (when w_{DMF} is above 0.70), the CTAB-coated GNRs are again stabilized and return to a well-dispersed state, because of the relatively poor solubility of the CTAB headgroup in the lower dielectric solvent mixture. We postulate that under these conditions, the GNRs may be encased in reverse micelles of CTAB.

The above result suggests that there exists an optimum window of solvent composition (w_{water} or $1-w_{DMF}$ = 0.30–0.70) in which the exchange between CTAB and BCP can take place on the surfaces of GNRs. To determine whether the PEO-PnBA polymers are inclined to aggregate into micellar structures in this same solvent composition range, we first investigated the self-assembly behavior of the PEO-PnBA diblock copolymer PEO_{113}–$PnBA_{89}$ as a function of water/DMF weight ratio. Figure S1 of the Supporting Information (SI) shows that DMF is a good solvent for both PEO_{113} and $PnBA_{89}$: in pure DMF, the block copolymer is fully dissolved and its size is undetectable by dynamic light scattering (DLS). When a small amount of water is added such that w_{water} = 0.05, the copolymer starts to aggregate into large but metastable colloidal particles. These grow over time when the solution is left quiescent, but can fragment into smaller particles with ultrasonication. This suggests that while the block copolymer molecules tend to aggregate at this solvent composition, they still have sufficient mobility to exchange between clusters at an appreciable rate. When the water content is increased to w_{water} = 0.10, submicrometer-sized micelles are observed whose sizes distributions are stable over time. This indicates that the

mobility of the BCP molecules is significantly reduced in more polar solvent mixtures, and suggests that a binary solvent composition with w_{water} = 0.05 would be optimal for exchanging CTAB with BCP molecules for stabilizing GNRs. Unfortunately, the solvent composition window for forming stable BCP micelles does not overlap well with the optimal solvent composition range for efficient CTAB exchange and displacement, established above.

To shift the BCP micellization window to a more polar solvent composition, we studied the self-assembly behavior of PEO_{113}–$PnBA_{57}$, which is more hydrophilic than PEO_{113}–$PnBA_{89}$. The reduced hydrophobic character of the $PnBA_{57}$ segment is expected to delay the onset of kinetic aggregation that occurs during the progressive addition of water into BCP solutions prepared in pure DMF, thereby shifting the window of stable micelle formation to higher values of w_{water}. As shown in Figure 2, when the water fraction is lowered, the metastable

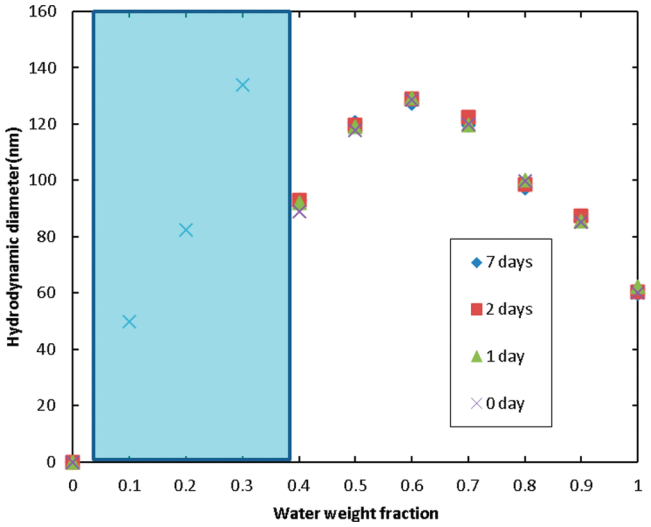

Figure 2. Mean hydrodynamic diameter of PEO_{113}–$PnBA_{57}$ BCP micelles in a water/DMF mixture, as a function of w_{water} and time. The shaded area represents a solvent composition window in which the BCP molecules aggregate into metastable colloids, signifying a medium for rapid exchange.

BCP clusters were not observed to form until $w_{water} \approx 0.4$, permitting an expansion in the solvent composition window for surfactant exchange and GNR encapsulation. This micellization processing window now has a considerable overlap with the solvent window for optimal CTAB exchange (i.e., $w_{water} \approx 0.30 - 0.40$).

On the basis of the data discussed above, we used PEO_{113}–$PnBA_{57}$ and a binary water/DMF solvent mixture with w_{water} = 0.35, to mediate the exchange and replacement of CTAB on the GNR surface with the BCP layer. The details of the surfactant exchange procedure are described in the Experimental Section. Briefly, a premade solution of CTAB-stabilized GNRs in a water/DMF mixture was first mixed with a separately prepared DMF solution of PEO_{113}–$PnBA_{57}$ to a final solvent composition of w_{water} = 0.35. After allowing time for the surfactant exchange process to occur at this solvent composition, an additional amount of water was added to help the BCP coating to become more compact. Afterward, the GNR suspension was dialyzed against deionized water to remove residual DMF and CTAB. This procedure allowed us to produce a BCP-coated GNR dispersion that is stable even under physiological NaCl concentrations for at least six months, as will be demonstrated in the next section.

2.3. Characterizations of the BCP-Encapsulated GNRs.

As shown in Figure 3 in the Supporting Information, the effective hydrodynamic diameter of the dialyzed PEO_{113}–$PnBA_{57}$-coated GNRs in water was determined to be about 40 nm, which did not change even after almost 7 months of storage. The zeta potential of the BCP-coated GNRs was −1.7 ± 1.1 mV, which suggests that a significant (if not all) amount of CTAB has been removed from the GNR surface by the surfactant exchange process (the zeta potential of the original CTAB-coated GNRs was +14.1 ± 0.46 mV).

The stability and hydrodynamic diameter of the BCP-encapsulated GNRs was also monitored by DLS in 150 mM NaCl, over *a* > 6-month period (Figure 3). This data indicates

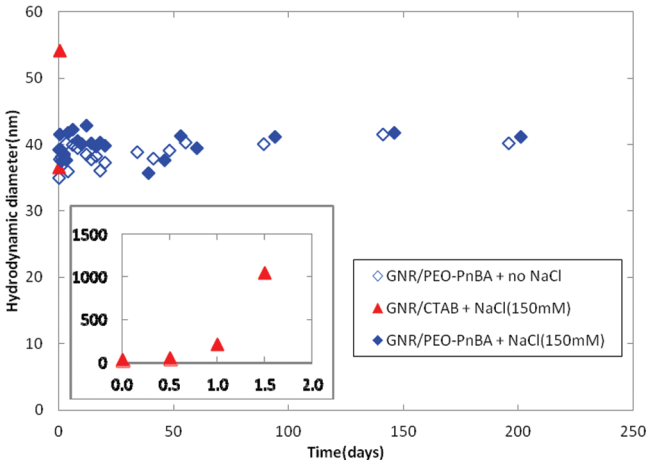

Figure 3. Mean hydrodynamic diameters (based on the intensity-weighted size distributions by DLS) of PEO_{113}–$PnBA_{57}$ BCP and CTAB-stabilized GNRs in pure water or in 150-mM NaCl solution, as a function of time. The BCP-coated GNRs are stable even at the high ionic strength (blue data points). The CTAB-coated GNRs undergo rapid aggregation at 150 mM NaCl (red data points), and the size of the aggregates becomes unmeasurable ($\gtrsim 3\ \mu m$) within less than 48 h. Two data points representing large-sized aggregates formed by the CTAB-coated GNRs were truncated to save space; a plot including all the data points for the CTAB GNR system over a shorter time period is shown in the inset of the figure. Representative DLS correlation functions and intensity-weighted size distributions (obtained by log-normal analysis) for these samples are presented in Figure S2 in the Supporting Information. The well-dispersed nature of the BCP-coated GNR samples and the aggregated nature of the CTAB-coated GNRs have been confirmed also by their respective optical absorbance spectra (data shown in Figure S3 in the Supporting Information).

that the BCP-coated GNRs are stable even at high ionic strength, implying that colloidal stability is derived from entropic steric repulsion provided by the polymer chains of the physisorbed BCP layer. In comparison, CTAB-coated GNRs are unstable under physiological salt conditions and undergo rapid aggregation, because of the screening of the electrostatic double layer provided by the CTAB coating. Although most of the CTAB can be replaced or covered by negatively charged polyelectrolytes such as polystyrenesulfonate (PSS), this has been shown to be insufficient to provide long-term stability to GNR dispersions.[2]

The widely used approach of passivating GNRs with thiol-functionalized PEO does not always completely displace the original CTAB coating, with the result being that the PEO-

grafted GNRs may not be fully inert to protein adsorption in physiological environments.[18] To validate the formation of a uniformly dense BCP coating on the GNR surface, transmission electron microscopy (TEM) images were acquired with uranyl acetate staining (see Figure 4). All GNRs in the TEM images were encapsulated by the BCP micelles (i.e., no uncoated particles were observed), indicating the BCP encapsulation process to be highly efficient. The negative contrast of the PnBA layer around an isolated GNR suggests a complete and uniform covering around the particle with a thickness of 7.3 ± 1.2 nm. From this data, we estimate that each BCP molecule covers an area of 1.4 nm^2 on the GNR surface, which translates into a normalized area of $\alpha/\pi R_{g,PEO}^2 \approx 0.14$ per PEO chain, where α denotes the coverage area per PEO chain and $R_{g,PEO}$ is the radius of gyration of the PEO block in the self-avoiding random-walk configuration (~26 Å based on previously reported parameters).[42] Our estimate suggests that the end-grafted PEO chains are extended in a polymer brush configuration ($\alpha/\pi R_{g,PEO}^2 < 1$), and can thus be expected to provide a complete passivation of GNRs against protein adsorption.[43]

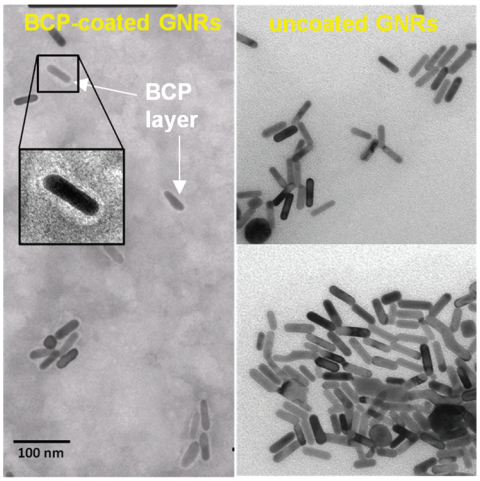

Figure 4. Representative transmission electron microscopy (TEM) images of (left) PEO_{113}–$PnBA_{57}$ BCP-coated GNRs (prepared by surfactant exchange at a solvent composition of w_{water} = 0.35, stored in pure water for 30 days after preparation) and (right) CTAB-coated GNRs (as synthesized in water), both negatively stained with (2%) uranyl acetate. Additional images of these samples are presented in Figures S4 and S5 of the Supporting Information.

Finally, we have also conducted BCP encapsulation trials at several other solvent compositions outside the determined range for optimal CTAB exchange (discussed in Section 2.2), i.e., at w_{water} = 0.20 and 0.50 with PEO_{113}–$PnBA_{57}$, and also at w_{water} = 0.05 with PEO_{113}–$PnBA_{89}$. The results of these tests (i.e., representative TEM micrographs of the respective BCP-treated GNR products) are presented, respectively, in Figures S6–S8 in the Supporting Information. As shown in these figures, the surfactant exchange processes undertaken outside the optimal solvency conditions failed to produce the desired encapsulation results.

3. CONCLUSION

GNRs can be efficiently encapsulated by PEO-PnBA BCP micelles using a simple solvent exchange method. The BCP-encapsulated GNRs are essentially devoid of CTAB and are stable against aggregation under physiological salt concentrations. We envision that the encapsulation process developed in this work can be scaled up for mass production, and can also be easily extended to the encapsulation and stabilization of other nanoparticle-based agents (e.g., magnetic metal-oxide nanoparticles) of current interest for medical imaging and hyperthermia applications.

4. EXPERIMENTAL SECTION

Materials. The PEO_{113}–$PnBA_{89}$ and PEO_{113}–$PnBA_{57}$ diblock copolymer samples were synthesized and characterized as described in our previous publications.[44−46] The polydispersity indices of these copolymers were determined (by gel permeation chromatography (GPC)) to be 1.15 (PEO_{113}–$PnBA_{89}$) and 1.15 (PEO_{113}–$PnBA_{57}$). GNRs were synthesized using the published procedure.[8] As shown in Figure 4, the GNR particles used have an average dimension of about 18 (cross-sectional diameter) by 50 (length) nm.

Surfactant Exchange Procedure. A solution of CTAB-stabilized GNRs (0.01 mg/mL) was initially dispersed in a water/DMF mixture with w_{water} = 0.70. A DMF solution of PEO_{113}–$PnBA_{57}$ (1.0 mg/mL) was prepared separately, then mixed in equal amounts with the GNR solution (each 1.0 mL) so that the final solvent composition contained a water weight fraction of 0.35. The mixture was sonicated for 30 min in a sonicating bath, then characterized by DLS. The mean hydrodynamic diameter of the (presumably BCP-coated) GNR particles was determined be about 85 nm. Water (0.6 mL) was added to a final solvent composition of w_{water} = 0.50, followed by another 30 min of sonication. This reduced the hydrodynamic diameter of the GNRs to about 75 nm, which suggests that the BCP coating became more compact under more polar solvent conditions. The GNR suspension was then purified by membrane dialysis (molecular weight cutoff 3,000) for 2 days against a large volume of deionized water to remove residual DMF and CTAB; 2.6 mL of the final GNR solution was obtained.

■ ASSOCIATED CONTENT

Supporting Information

Mean diameter of PEO_{113}–$PnBA_{89}$ BCP micelles as a function of water/DMF weight ratio (Figure S1); DLS correlation functions and intensity-weighted size distributions for various GNR samples (Figure S2); UV–vis absorption spectra for various GNR samples (Figure S3); additional TEM images of PEO_{113}–$PnBA_{57}$ BCP-coated GNRs (Figure S4); additional TEM images of CTAB-coated GNRs (Figure S5); TEM images demonstrating unsuccessful BCP encapsulation trials conducted at solvent compositions outside the optimal process window (Figures S6–S8). This material is available free of charge via the Internet at http://pubs.acs.org.

■ AUTHOR INFORMATION

Corresponding Author

*E-mail: yywon@ecn.purdue.edu.

Notes

The authors declare no competing financial interest.

■ ACKNOWLEDGMENTS

Y.Y.W. thanks the 3M Company for the Nontenured Faculty Award, and also the National Science Foundation (NSF) for a grant (DMR-0906567), from which a small fraction of the expenses of this work were defrayed. The authors also gratefully acknowledge financial support from KCC Corporation (Korea) for DHK's graduate studies.

REFERENCES

(1) Huang, X. H.; Neretina, S.; El-Sayed, M. A. *Adv. Mater.* **2009**, *21* (48), 4880−4910.
(2) Leonov, A. P.; Zheng, J. W.; Clogston, J. D.; Stern, S. T.; Patri, A. K.; Wei, A. *ACS Nano* **2008**, *2* (12), 2481−2488.
(3) Bogliotti, N.; Obereitner, B.; Di-Cicco, A.; Schmidt, F.; Florent, J. C.; Semetey, V. *J. Colloid Interface Sci.* **2011**, *357* (1), 75−81.
(4) Link, S.; Mohamed, M. B.; El-Sayed, M. A. *J. Phys. Chem. B* **1999**, *103* (16), 3073−3077.
(5) Link, S.; El-Sayed, M. A. *Int. Rev. Phys. Chem.* **2000**, *19* (3), 409−453.
(6) Tong, L.; Wei, Q. S.; Wei, A.; Cheng, J. X. *Photochem. Photobiol.* **2009**, *85* (1), 21−32.
(7) Murphy, C. J.; Thompson, L. B.; Chernak, D. J.; Yang, J. A.; Sivapalan, S. T.; Boulos, S. P.; Huang, J. Y.; Alkilany, A. M.; Sisco, P. N. *Curr. Opin. Colloid Interface Sci.* **2011**, *16* (2), 128−134.
(8) Nikoobakht, B.; El-Sayed, M. A. *Chem. Mater.* **2003**, *15* (10), 1957−1962.
(9) Huff, T. B.; Hansen, M. N.; Zhao, Y.; Cheng, J. X.; Wei, A. *Langmuir* **2007**, *23* (4), 1596−1599.
(10) Balasubramanian, S. K.; Jittiwat, J.; Manikandan, J.; Ong, C. N.; Yu, L. E.; Ong, W. Y. *Biomaterials* **2010**, *31* (8), 2034−2042.
(11) Yu, C. X.; Varghese, L.; Irudayaraj, J. *Langmuir* **2007**, *23* (17), 9114−9119.
(12) Rostro-Kohanloo, B. C.; Bickford, L. R.; Payne, C. M.; Day, E. S.; Anderson, L. J. E.; Zhong, M.; Lee, S.; Mayer, K. M.; Zal, T.; Adam, L.; Dinney, C. P. N.; Drezek, R. A.; West, J. L.; Hafner, J. H. *Nanotechnology* **2009**, *20* (43).
(13) Chang, A.; Enoch, J. M.; Seu, J.; Ling, D.; Le, D. A.; Lakshminarayanan, V.; Choi, S. *Invest. Ophth.Vis. Sci.* **2004**, *45*, U1001−U1001.
(14) Chang, J. Y.; Wu, H. M.; Chen, H.; Ling, Y. C.; Tan, W. H. *Chem. Commun.* **2005**, *8*, 1092−1094.
(15) Pierrat, S.; Zins, I.; Breivogel, A.; Sonnichsen, C. *Nano Lett.* **2007**, *7* (2), 259−263.
(16) Gole, A.; Murphy, C. J. *Chem. Mater.* **2005**, *17* (6), 1325−1330.
(17) Pastoriza-Santos, I.; Perez-Juste, J.; Liz-Marzan, L. M. *Chem. Mater.* **2006**, *18* (10), 2465−2467.
(18) Grabinski, C.; Schaeublin, N.; Wijaya, A.; D'Couto, H.; Baxamusa, S. H.; Hamad-Schifferli, K.; Hussain, S. M. *ACS Nano* **2011**, *5* (4), 2870−2879.
(19) Kumar, A.; Whitesides, G. M. *Abstr. Pap. Am. Chem. Soc.* **1993**, *206*, 172-COLL.
(20) Liu, Y. L.; Shipton, M. K.; Ryan, J.; Kaufman, E. D.; Franzen, S.; Feldheim, D. L. *Anal. Chem.* **2007**, *79* (6), 2221−2229.
(21) Caswell, J. L.; Kesteven, M. J.; Komesaroff, M. M.; Haynes, R. F.; Milne, D. K.; Stewart, R. T.; Wilson, S. G. *Mon. Not. R. Astron. Soc.* **1987**, *225* (2), 329−334.
(22) Caswell, K. K.; Wilson, J. N.; Bunz, U. H. F.; Murphy, C. J. *J. Am. Chem. Soc.* **2003**, *125* (46), 13914−13915.
(23) Thomas, K. G.; Barazzouk, S.; Ipe, B. I.; Joseph, S. T. S.; Kamat, P. V. *J. Phys. Chem. B* **2004**, *108* (35), 13066−13068.
(24) Thierry, B.; Ng, J.; Krieg, T.; Griesser, H. J. *Chem. Commun.* **2009**, *13*, 1724−1726.
(25) Bhatt, N.; Huang, P. J. J.; Dave, N.; Liu, J. W. *Langmuir* **2011**, *27* (10), 6132−6137.
(26) Won, Y. Y.; Bates, F. S. Nonionic Block Copolymer Wormlike Micelles. In *Giant Micelles: Properties and Applications*; Zana, R., Kaler, E. W., Eds.; CRC Press-Taylor & Francis Group: Boca Raton, FL, 2007; Vol. *140*, pp 417−451.
(27) Gohy, J. F. Block copolymer micelles. In *Block Copolymers II*; Abetz, V., Ed.; Springer-Verlag: Berlin, 2005; Vol. *190*, pp 65−136.
(28) Won, Y. Y.; Davis, H. T.; Bates, F. S. *Macromolecules* **2003**, *36* (3), 953−955.
(29) Chen, Y.; Cho, J.; Young, A.; Taton, T. A. *Langmuir* **2007**, *23* (14), 7491−7497.
(30) Kang, Y. J.; Taton, T. A. *Angew. Chem., Int. Ed.* **2005**, *44* (3), 409−412.
(31) Tan, L. H.; Xing, S. X.; Chen, T.; Chen, G.; Huang, X.; Zhang, H.; Chen, H. Y. *ACS Nano* **2009**, *3* (11), 3469−3474.
(32) Yang, M. X.; Chen, T.; Lau, W. S.; Wang, Y.; Tang, Q. H.; Yang, Y. H.; Chen, H. Y. *Small* **2009**, *5* (2), 198−202.
(33) Kamps, A. C.; Sanchez-Gaytan, B. L.; Hickey, R. J.; Clarke, N.; Fryd, M.; Park, S. J. *Langmuir* **2010**, *26* (17), 14345−14350.
(34) Ai, H.; Flask, C.; Weinberg, B.; Shuai, X.; Pagel, M. D.; Farrell, D.; Duerk, J.; Gao, J. M. *Adv. Mater.* **2005**, *17*, (16), 1949−1952.
(35) Lecommandoux, S. B.; Sandre, O.; Checot, F.; Rodriguez-Hernandez, J.; Perzynski, R. *Adv. Mater.* **2005**, *17*, (6), 712-+.
(36) Parthiban, A.; Likhitsup, A.; Choo, F. M.; Chai, C. L. L. *Polym. Chem.* **2010**, *1* (3), 333−338.
(37) Lendlein, A.; Schmidt, A. M.; Langer, R. *Proc. Natl. Acad. Sci. U.S.A.* **2001**, *98* (3), 842−847.
(38) Roff, W. J., *Handbook of Common Polymers: Fibres, Films, Plastics, and Rubbers*; CRC Press: Boca Raton, FL, 1971.
(39) Nikoobakht, B.; El-Sayed, M. A. *Langmuir* **2001**, *17* (20), 6368−6374.
(40) Lyklema, J.; Leeuwen, H. P. v.; Vliet, M. v.; Cazabat, A. M., *Fundamentals of Interface and Colloid Science*. Academic Press: London, 1991; p v.
(41) Lin, J.; Zhou, W. L.; O'Connor, C. J. *Mater. Lett.* **2001**, *49* (5), 282−286.
(42) Hiemenz, P. C.; Lodge, T., *Polymer Chemistry*, 2nd ed.; CRC Press: Boca Raton, FL, 2007; p 224.
(43) Waguespack, Y. Y.; Banerjee, S.; Ramannair, P.; Irvin, G. C.; John, V. T.; McPherson, G. L. *Langmuir* **2000**, *16* (7), 3036−3041.
(44) Sharma, R.; Goyal, A.; Caruthers, J. M.; Won, Y. Y. *Macromolecules* **2006**, *39* (14), 4680−4689.
(45) Sharma, R.; Lee, J. S.; Bettencourt, R. C.; Xiao, C.; Konieczny, S. F.; Won, Y. Y. *Biomacromolecules* **2008**, *9* (11), 3294−3307.
(46) Gary, D. J.; Lee, H.; Sharma, R.; Lee, J. S.; Kim, Y.; Cui, Z. Y.; Jia, D.; Bowman, V. D.; Chipman, P. R.; Wan, L.; Zou, Y.; Mao, G. Z.; Park, K.; Herbert, B. S.; Konieczny, S. F.; Won, Y. Y. *ACS Nano* **2011**, *5* (5), 3493−3505.
(47) Kwei, T. K.; Wang, T. T. *Abstr. Pap. Am. Chem. Soc.* **1974**, 50−50.
(48) Dann, J. R. *J. Colloid Interface Sci.* **1970**, *32*, (2), 302−320.
(49) Aqra, F.; Ayyad, A. *Appl. Surf. Sci.* **2011**, *257* (15), 6372−6379.
(50) Wu, S., *Polymer Interface and Adhesion*; Marcel Dekker: New York, 1982.